Hindawi
Modelling and Simulation in Engineering
Volume 2024, Article ID 6626705, 21 pages
https://doi.org/10.1155/2024/6626705

Research Article

Modeling and Parametric Analysis of a Large-Scale Solar-Based Absorption Cooling System

Ali Abdullah and Abdullah A. AlZahrani

Department of Mechanical Engineering, Umm Al-Qura University, Makkah, PO Box 715, Saudi Arabia

Correspondence should be addressed to Abdullah A. AlZahrani; aarzahrani@uqu.edu.sa

Received 21 August 2023; Revised 1 November 2023; Accepted 2 December 2023; Published 23 January 2024

Academic Editor: Vijayanandh Raja

This study investigates the thermodynamic performance of a solar-powered absorption cooling system. The system uses a lithium bromide-water (LiBr-H_2O) absorption refrigeration system (ARS) integrated with evacuated solar collectors (ETSC) and thermal energy storage (TES) to provide a 3 kTR cooling capacity for a university campus. The paper examines the performance of the integrated system under different design and operating conditions as well as the performance of each subsystem, i.e., ETSC, TES, and ARS. Furthermore, a parametric energy and exergy analysis is applied, where different parameters are studied, such as the temperatures of the generator, the condenser, the evaporator, and the absorber. In addition, the system performance is examined with the variation in environmental conditions. The coefficient of performance (COP), exergetic efficiency, exergy destruction, and fuel depletion ratio (FDR) are used to evaluate the system's performance. The ETSC and the TES are studied under the variation in solar radiation through the day in two seasons: summer and winter. The results revealed that the increase in generator temperature positively impacts the COP of the ARS while lowering the condenser and absorber temperature gives the same positive effect. Furthermore, the main reason for the exergy destruction is found to be the solar collector, which is responsible for destroying 89% of the input solar exergy. Additionally, 4.7% of the inlet exergy is destroyed in the generator, which makes 4.5% of the total exergy loss. The TES destroyed 4.8% of the total solar exergy input. The energy analysis shows that the ARS achieves an energetic COP of about 0.77, while the exergy analysis revealed that the exergetic COP is 0.21.

1. Introduction

Many factors, such as the fast rise in energy costs, supply security concerns, pollutant emissions, and global climate change, have all rendered current refrigeration systems unsustainable [1]. Concerns about the continuous use of traditional refrigeration systems and their environmental implications, such as ozone layer depletion and global warming, are growing. As an alternative, environmentally friendly refrigeration systems must be taken into consideration. Absorption systems use low-grade heat to produce a cooling effect. The required heat can be provided from renewable sources to reduce electricity demand and cost made by conventional vapor-compression systems.

In this regard, enhancing absorption refrigeration systems (ARS) has been one area of attention [2]. Ammonia-water and water-LiBr have become the most effective working fluid pairings in the majority of ARS applications [3]. However, water-LiBr solution has a lower environmental effect compared to vapor compression and NH_3-H_2O absorption systems [4].

Solar energy has many advantages over other energy sources because it is abundant and clean. However, solar energy is intermittent, and energy storage is required to provide energy from solar continuously [5]. Solar collectors are heat exchanger technology that were developed to efficiently capture solar thermal energy. However, it still needs further improvement and development, which has attracted the interest of scientists over the past few decades [6]. Evacuated tube solar collector (ETSC) is one option of the mature solar collector technologies, in which a vacuum is created between the absorber and the glass cover, which enables higher thermal efficiency compared with flat plate solar collectors. This vacuum gap lowers the convectional and conductional heat losses from the collector. Lower heat losses in the evacuated tube solar collectors led to higher working liquid outlet temperatures. Higher temperatures and pressures are more valuable for industrial applications, so ETSC would be preferable [7].

Several studies have been conducted using an exergy-based analysis to assess the performance of absorption refrigeration systems (ARS) [8]. For example, Gomri [9] used the first and the second laws of thermodynamics to analyze the changes in the coefficient of performance (COP), exergetic efficiency, and exergy destruction of the components of the system. The results showed an increase in the COP with the rise of the generator and evaporator temperatures and a decrease with the rise of the condenser temperature. An exergy-based thermoeconomic approach was applied to a single-effect H_2O-LiBr absorption system for air-conditioning purposes [10]. Şencan et al. [11] present a thermodynamic analysis of LiBr-H_2O absorption system for cooling where the exergy loss was calculated alongside COP and exegetic efficiency, focusing on the effect of the heat source temperature on the system performance. Kaynakli and Kilic [12] applied energy and exergy analyses to evaluate the performance of an H_2O-LiBr ARS. The effectiveness of the heat exchanger and the operating conditions were studied for their influence on system COP. According to their findings, COP increases as generator and evaporator temperatures rise and decreases as condenser and absorber temperatures rise. Kaushik and Arora [13] designed an H_2O-LiBr ARS with a series flow double effect and evaluated it using energy and exergy calculations. The outcomes were contrasted with a single-effect ARS, and energy and exergy studies were used to investigate the impact of operating conditions on the efficiency of the heat exchanger and ARS components. Rivera et al. [14] investigated the exergy and energy performance of an experimental single-effect LiBr-H_2O system, and they found that the maximum values of COP and exergetic coefficient of performance (ECOP) are achieved at the highest solution concentrations, while the cycle's improvement potential and exergy destruction stay essentially constant about the main operation parameters. Also, it was demonstrated that the COP and ECOP fall as absorber temperature rises while the improvement potential and the exergy destruction rise. Modi et al. [15] developed a numerical program to calculate the energy and exergy of a single-effect ARS. Their results show that at 87°C, the generator achieves its optimal COP and exergetic efficiency values of 0.74 and 25%, respectively. Kaynakli et al. [16] presented a thermodynamic simulation for a double-effect H_2O-LiBr ARS. They examined the impact of operating temperatures on the heat capacity and exergy destruction of the high-pressure generator, the overall system COP, and the mass flow rates of three various heat sources. They reported that the exergy destruction rate increases with increasing the heat source temperature while raising the temperature of the high-pressure generator leads to a decrease in its exergy destruction rate. Mohtaram et al. [17] used the exergy concept to investigate the performance of a lithium bromide ARS. The result showed that the absorber has the highest exergy destruction rate reaching 35% of the whole exergy destruction. Ahmad et al. [18] apply an energy analysis for single ARS for LiBr-H_2O and lithium chloride-water (LiCl-H2O) with different operational parameters, and their result shows that the LiBr-H2O system's maximum COP is found to be between 0.741 and 0.902, whereas the LiCl-H2O system's maximum COP is between 0.809 and 0.926.

The development of an effective connection between solar energy collecting and the absorption unit has been the subject of several research studies [19, 20]. Leonzio [21] presents a thermodynamic analysis on the performance of solar-powered LiBr-H_2O ARS used to extract water from the air. They observed that the largest water output occurs in January owing to the comparatively high relative humidity, while the maximum cooling production occurs in July due to the high solar radiation. Similarly, the performance of a solar-aided absorption heat pump system with a 100 kW cooling capacity was presented by Ileri [22]. He reported that the COP gives inaccurate guidance on how to set the reference temperature in both the winter and the summer, whereas FNP (the fraction of nonpurchased energy) offers a more meaningful measure than the COP. Rezaie et al. [23] studied the exergy and energy performance of thermal energy storage in a district energy system to enhance the effectiveness of solar collectors. They found that the overall exergy and energy efficiencies are 19% and 60%, respectively. A solar-powered LiBr-H_2O absorption refrigeration system of 10-ton cooling capacity was studied by Pongtornkulpanich et al. [24]. They showed that 81% of the chiller's annual average thermal energy needs were met by the 72 m^2 evacuated tube solar collector, while the remaining 19% was covered by an LPG- (liquefied petroleum gas-) fired backup heater. Onan et al. [25] applied an exergy analysis on a solar-driven absorption cooling system and studied the exergy loss on an hourly basis. The solar collectors and generator were found to obtain most of the system's energy losses. Exergy loss varies between 5% and 8% in the generator and 10% and 70% in the collector. Sumathy et al. [26] developed an integrated solar ARS system for air-conditioning purposes. They found that the maximum exergetic efficiency of the solar collector and the ARS can be achieved when ARS is supplied with a hot fluid temperature between 70 and 80°C with an inlet temperature between 65 and 75°C for the solar collector. Kerme et al. [27] applied an exergy and energy analysis on a solar-powered H_2O-LiBr ARS combined with a flat plate collector; it was noticed that the increase in the inlet generator temperature resulted in a slight increase in the COP and increase in the exergy loss for the ARS component, and most of the exergy losses was done by the solar collector. Rosiek [28] investigated a solar-powered single-effect H_2O-LiBr ARS in which the best result from an exergetic approach can be obtained with a temperature range between 70 and 80°C supplied to the ARS with the support of two chilled water tanks.

From the previous literature, one can realize the role that absorption systems play in replacing the conventional cooling systems that are responsible for consuming large

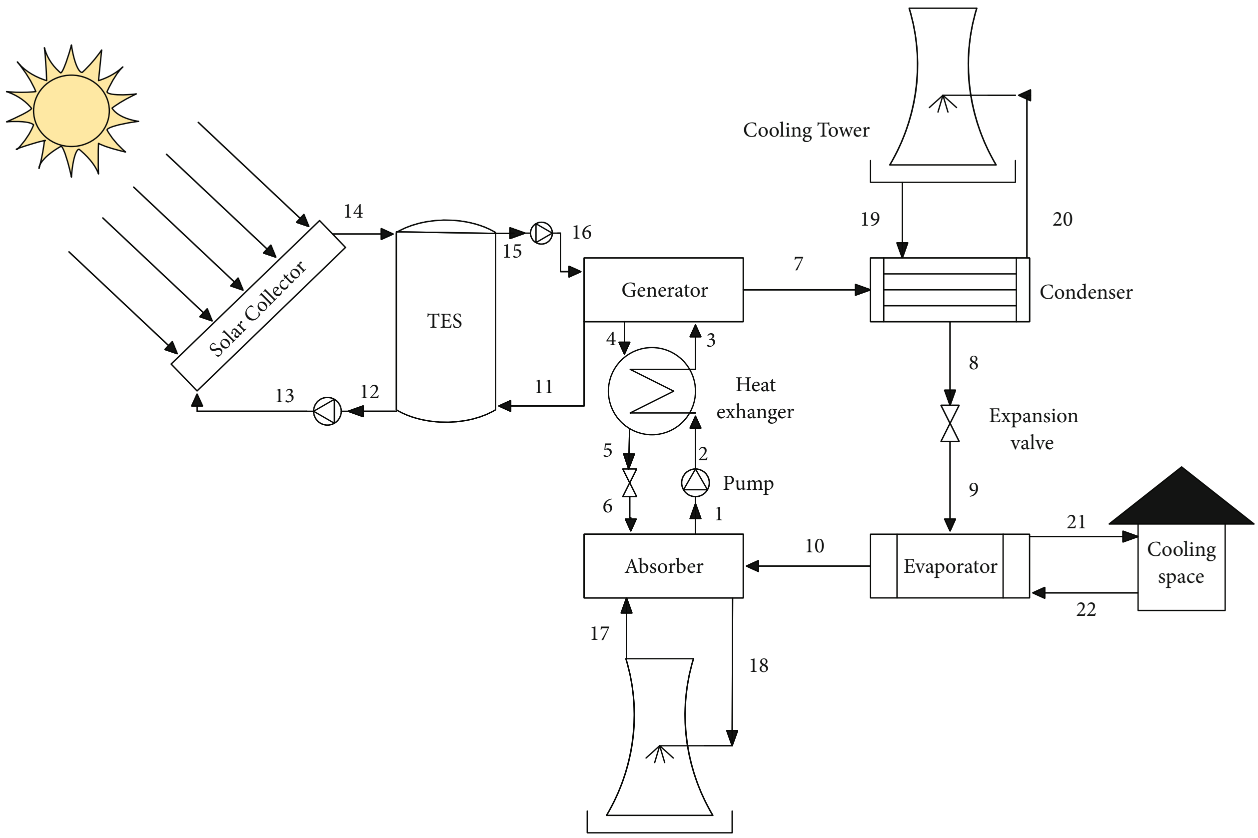

FIGURE 1: Schematic diagram for the solar-powered LiBr-H_2O ARS.

amounts of electricity, especially in countries with large cooling loads such as Saudi Arabia, in which cooling load can reach as much as 70% in some cities. Therefore, the current work investigates using an H_2O-LiBr absorption system powered by solar energy to replace a conventional large-scale vapor-compression system used for a university campus to provide cooling. Although the exergy analysis of single-effect absorption refrigeration systems has been the subject of several scientific studies, the current study contributes to multiple areas that have been overlooked in the previous studies. The contributions of this work can be summarized in the following points:

(i) The current analysis considered the designing and optimization of the entire system based on the second law, i.e., the exergy efficiency

(ii) The effective integration and modeling of the TES are considered to achieve continuous operation maintaining the ARS system operation day and night when needed

(iii) The actual weather data for the representative days for summer and winter in a typical high-cooling load city in Saudi Arabia is considered

(iv) The detailed system exergetic performance is presented and discussed for the entire system as well as each component of the system

2. System Description

A solar-driven single-effect lithium bromide was presented in this project, a traditional ARS with the main component's absorber, generator, condenser, evaporator, heat exchanger, solution pump, and expansion valve supported with evacuated tube solar collector as a heat source, thermal storage for the storing process, and two cooling towers for heat reject. The system is designed to provide a desired cooling/refrigeration load of three tons of refrigeration with no emission alongside the process for environmental care.

2.1. Solar-Evacuated Tube. An evacuated solar collector is integrated with the ARS, as shown in Figure 1, where the Syltherm 800 (heat transfer fluid) [29] is circulated between the ETSC and TES, and the solar energy absorbed by the collectors is transformed into heat energy in (13) and (14). ETSC was selected for this design because of the need for a higher temperature than a flat plat collector can achieve [30]. Syltherm 800 was selected as the solar system thermal oil due to the need for a higher temperature exceeding 100°C, so water was not an option. The input data for the sun radiation was taken for 24 hours on 23 June 2002 for the summer case and on 11 December for the winter case by NREL and KACST for Al-Madinah City in Saudi Arabia (see Table 1). In Table 2, the performance parameters of the ETSC are listed. Figure 2 shows the sectional view of the ETSC.

Table 1: Location and average data for Al-Madinah City on 23 June (Aljeddani [43]; NERL [44]).

Direct normal radiation	984.3 W/m^2
Latitude	24.55 N
Altitude	39.70 E
Average relative humidity	19.5%
Average ambient temperature	32.5°C
Extreme ambient temperature	38°C
Lowest ambient temperature	26.6°C

Table 2: Parameters of the evacuated tube solar collector.

Input parameters	Values
$F_R U_l$ [22]	3.3 (W/m^2 °C)
$F_R(\alpha\tau)$ [22]	0.7
T_{in}	90°C
T_{out}	120°C

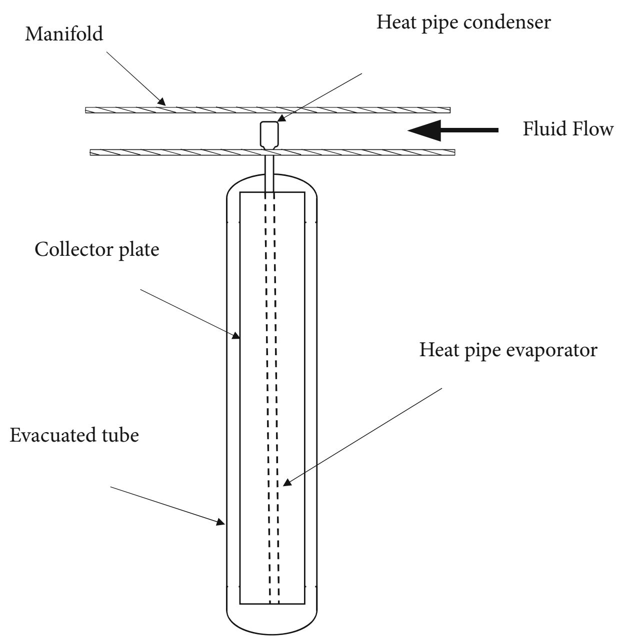

Figure 2: Evacuated tube collector diagram [31].

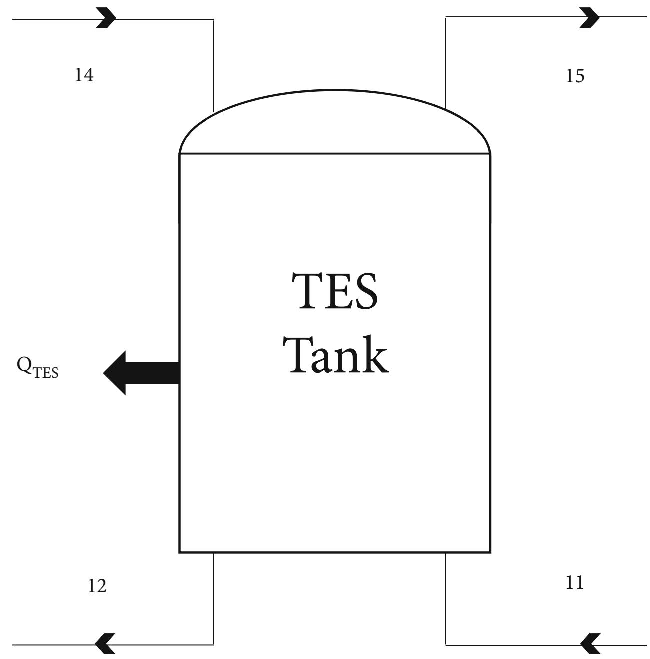

Figure 3: Thermal energy storage tank diagram.

2.2. TES. The absorption cooling system is supported by a thermal storage tank to store the solar energy captured and offer continuous heat supply when there is not enough sun radiation to ensure the system operates continuously for 24 hours. The fluid within the insulated storage tank is assumed to be fully mixed with the water returning to the tank from the collector and the generator to simplify the model. As shown in Figures 1 and 3, TES gets the energy from the solar collector (14, 13) and supplies the generator with the energy needed (15, 11).

2.3. ARS. The single-effect lithium bromide ARS consists of an absorber, generator, condenser, evaporator, heat exchanger, solution pump, and expansion valve. As shown in Figures 1 and 4, the generator is provided with the high temperature from the TES (11 and 16), which led to an increase in the lithium bromide solution temperature where the water vapor is driven out of the solution at (7), leaving as a strong solution [4] of LiBr. The condenser cools down the superheated vapor temperature and condenses it to a saturated liquid state (8). The liquid enters the evaporator after passing through the throttle valve, where the pressure drops (9). Then, the water (refrigerant) is transferred from the evaporator to the absorber as a saturated vapor, where it is absorbed by the LiBr solution (10) and then pumped up to a higher pressure through the pump (1) and then boiled out of the solution due to the increase in the heat added through the process (2 and 3). Simultaneously, the strong solution in the generator (4) returns to the heat exchanger and passes via the throttle valve toward the absorber (5 and 6). In Table 3, the reference case input parameters are provided.

2.4. Cooling Towers. The system is backed up with two cooling towers that were added to the cycle connected to the condenser and absorber where the heat rejected through the water circulates between them and both the condenser and absorber (17, 18, 19, and 20) to enhance the system performance by increasing both heat rejection for the condenser and the absorber in parallel. The cooling tower's design temperature ranges between 30 and 35°C, based on standard absorption chiller specifications [32].

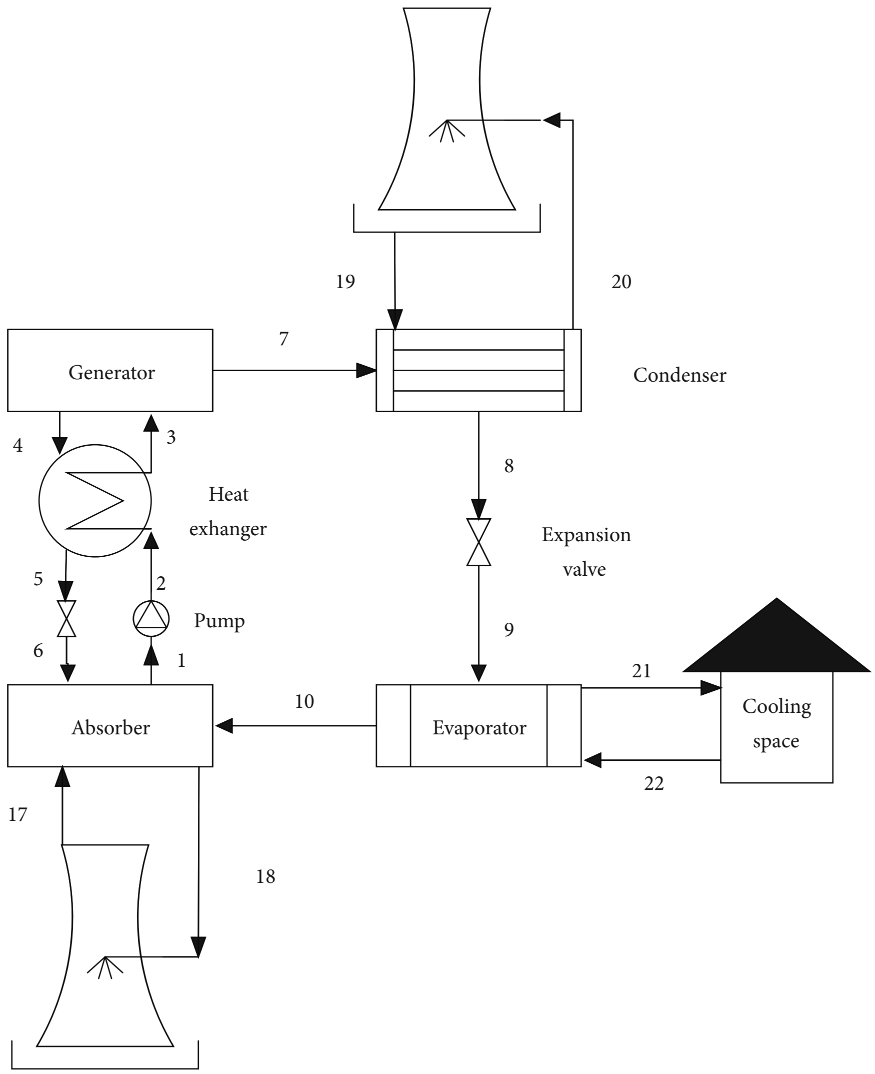

Figure 4: Schematic diagram of the ARS and the cooling towers.

Table 3: Baseline input data are used to analyze solar-powered LiBr-H_2O ARS.

Input parameters	Values
$T_{cond} = T_{abs}$	40°C
T_{eva}	10°C
T_{gen}	95°C
Generator inlet temperature T_{16}	110°C
Effectiveness of solution heat exchanger [42]	0.64
Cooling capacity (Q_{eva})	3000 TR

3. Energy and Exergy Analysis

For the sake of system modeling and performance evaluation, the following assumptions are made in addition to the details provided in the system description section:

(i) All the components of the ARS operate in a steady-state condition

(ii) The friction and pressure losses within the pipes are negligible

(iii) The refrigerant phase is saturated liquid at the condenser outlet and saturated vapor at the evaporator output

(iv) The changes in chemical exergy are neglected, as no chemical reactions are involved

(v) The dead-state conditions for the environment are taken at 25°C and 1 atm pressure

(vi) The weak solution leaves the absorber at the absorber temperature. Similarly, the strong solution leaves the generator at the generator temperature

(vii) The convection heat losses due to wind from the ETSC surface are neglected

(viii) The cooling tower operating temperatures range between 30 and 35°C [32]

The general energy balance equation for a control volume, under steady-state conditions, can be expressed in the following:

$$\dot{Q}_{\text{in}} + \dot{W}_{\text{in}} + \sum_{\text{in}} \dot{m}h = \dot{Q}_{\text{out}} + \dot{W}_{\text{out}} + \sum_{\text{out}} \dot{m}h. \quad (1)$$

Refrigerant mass flow rate m_{ref} is calculated from the following equation of the evaporator:

$$\dot{m}_{\text{ref}} = \frac{\dot{Q}_{\text{eva}}}{(h_{10} - h_9)}. \quad (2)$$

The cooling water mass flow rate $\dot{m}_w$ is calculated by applying energy balance on the evaporator and condenser.

$$\dot{m}_w = \frac{\dot{Q}}{(h_{\text{in}} - h_{\text{out}})}. \quad (3)$$

For the cooling tower, the air and makeup water mass flow rates $\dot{m}_{\text{air}}$ are calculated as follows:

$$\dot{m}_{\text{air}} = \frac{\dot{m}_{w,5}(h_5 - h_6)}{(h_{\text{air},2} - h_{\text{air},1}) - (\omega_2 - \omega_1)h_6}. \quad (4)$$

Equations for exergy destruction for the system components are shown as follows:

The exergy at any point can be defined as the following [33]:

$$\text{ex} = (h - h_0) - T_0(s - s_0). \quad (5)$$

The exergy destruction rate of a control volume at a steady state for each component of the system can be defined as follows [10]:

$$E = \sum_{\text{in}} \dot{m}\text{ex} - \sum_{\text{out}} \dot{m}\text{ex} + \sum \dot{Q}\left(1 - \frac{T_0}{T}\right) - \dot{W}, \quad (6)$$

where E represents the exergy loss throughout the process or any irreversibility that was placed. The exergy of the input and outflow streams of the control volume is the first two terms on the right side of Equation (6). The third and fourth terms represent the exergy connected to the heat transmitted from the source while conserving it at a constant temperature T. The final term is the mechanical work exergy added to the control volume.

3.1. Solar-Evacuated Tube. The application of energy and exergy balance equations represents the basic thermodynamic modeling of an ETSC. The equations for an ETSC in a steady state for energy and exergy were collected from Eltaweel et al. [34], Kalogirou et al. [35], and Duffie and Beckman [36]. The balance equation of energy is given by

$$\dot{Q}_u = \dot{Q}_{\text{Abs}} - \dot{Q}_{\text{loss}}, \quad (7)$$

where $\dot{Q}_u$ is the useful energy gain and $\dot{Q}_{\text{Abs}}$ is the absorbed solar radiation from which losses $\dot{Q}_{\text{loss}}$ have been subtracted where the losses happen due to the conduction, convection, and radiation between the collector and the atmosphere.

The loss can be calculated by

$$\dot{Q}_{\text{loss}} = F_R U_l A_c (T_{\text{in}} - T_a). \quad (8)$$

The useful energy is described as

$$\dot{Q}_u = \text{A}_c F_R [I(\alpha\tau) - U_l (T_{\text{in}} - T_a)]. \quad (9)$$

The thermal efficiency of the collector is given by

$$\eta_c = \frac{\dot{Q}_u}{\text{A}_c * I}. \quad (10)$$

The exergy destruction rate within the PTC can be calculated using

$$\dot{E}_{\text{ETSC}} = m_{\text{solar}}(E_{13} - E_{14}) + \dot{E}x_s - \dot{E}x_L. \quad (11)$$

The exergy of incident solar energy can be determined according to

$$\dot{E}x_s = \dot{Q}_{\text{Abs}} \left\{ 1 - \frac{4}{3} * \left(\frac{T_a}{T_s}\right) + \frac{1}{3} * \left(\frac{T_a}{T_s}\right)^4 \right\}, \quad (12)$$

where T_s is the solar surface temperature, which is taken as 5777 K. The exergy loss can be represented as

$$\dot{E}x_L = \dot{Q}_{\text{loss}} \left(1 - \frac{T_0}{T_r}\right). \quad (13)$$

The exergy efficiency can be represented as

$$\eta_{II-\text{ETSC}} = \frac{m_{\text{solar}}(E_{13} - E_{14})}{\dot{E}x_s}. \quad (14)$$

3.2. TES. An energy and exergy balance for a thermal system can be written according to Dinçer and Rosen [37].

The energy balance is described as

$$\text{Energy input} - \text{energy output} = \text{energy accumulation},$$
$$Q_{\text{in-TES}} - (Q_{\text{out-TES}} + Q_{\text{loss-TES}}) = \Delta E. \quad (15)$$

The exergy balance can be obtained as follows:

$$\begin{aligned}&\text{Exergy input} - \text{exergy output} - \text{exergy consumption}\\&\quad = \text{exergy accumulation},\\&\quad \mathrm{Ex}_{\text{in-TES}} - (\mathrm{Ex}_{\text{out-TES}} + \mathrm{Ex}_{\text{loss-TES}}) - I = \Delta\mathrm{Ex}.\end{aligned} \tag{16}$$

The calculation for the total mass of the TES is

$$\dot{Q}_{\text{in}} = m_{\text{tes}} * (h_{15} - h_{11}). \tag{17}$$

Energy is transported to and from the TES with water. The mass which flows during charging can be written as follows:

$$m_{\text{TES},c} = \frac{Q_{\text{in-TES}}}{C_p(T_{14} - T_{13})}. \tag{18}$$

The mass which flows during discharging can be written as follows:

$$m_{\text{TES},d} = \frac{Q_{\text{out-TES}}}{C_p(T_{15} - T_{11})}. \tag{19}$$

The energy loss to the ambient surroundings can be obtained as follows [38]

$$Q_{\text{loss-TES}} = UA\,(T_{14} - T_0). \tag{20}$$

Here the TES overall heat transfer coefficient is taken as 11.1?W/K [27]. If $Q_{\text{in-TES}}$ and $Q_{\text{out-TES}}$ are considered constant with the loss over a time period Δt, the TES temperature can be expressed as [36, 39]

$$T_{\text{tes,new}} = T_{\text{tes}} + \frac{\Delta t}{mCp}\left[Q_{\text{in-TES}} - Q_{\text{out-TES}} - UA\,(T_{\text{tes}} - T_0)\right], \tag{21}$$

where $T_{\text{tes,new}}$ is the liquid final temperature in TES at the end of the time interval Δt.

The exergy loss is expressed as

$$\mathrm{Ex}_{\text{loss-TES}} = \dot{Q}_{\text{loss-TES}}\left(1 - \frac{T_0}{T_{\text{avg}}}\right). \tag{22}$$

The exergy accumulation is expressed as

$$\Delta\mathrm{Ex} = \mathrm{Ex}_f - \mathrm{Ex}_i. \tag{23}$$

The input exergy equation is expressed as

$$\mathrm{Ex}_{\text{in-TES}} = m_{\text{TES}c}\,(\mathrm{ex}_{14} - \mathrm{ex}_{13}). \tag{24}$$

The exergy destruction for the TES is obtained as

$$I = \mathrm{Ex}_{\text{in-TES}} - (\mathrm{Ex}_{\text{out-TES}} + \mathrm{Ex}_{\text{loss-TES}}) - \Delta\mathrm{Ex}. \tag{25}$$

The energy efficiency can be defined as

$$\eta_{\text{TES}} = \frac{Q_{\text{out-TES}}}{Q_{\text{in-TES}}}. \tag{26}$$

The exergy efficiency can be defined as

$$\eta_{\text{ex-TES}} = \frac{\mathrm{Ex}_{\text{out-TES}}}{\mathrm{Ex}_{\text{in-TES}}}. \tag{27}$$

3.3. ARS. The absorber energetic balance is given as

$$\dot{Q}_{\text{ab}} = \dot{m}_{10} * h_{10} + \dot{m}_6 * h_6 - \dot{m}_1 * h_1 = \dot{m}_{13}\,(h_{18} - h_{17}). \tag{28}$$

The condenser energetic balance is given as

$$\dot{Q}_{\text{con}} = \dot{m}_7 * h_7 - \dot{m}_8 * h_8 = \dot{m}_{20}\,(h_{20} - h_{19}). \tag{29}$$

The heat exchanger energetic balance is given as

$$\dot{Q}_{\text{HX}} = \dot{m}_3 * h_3 - \dot{m}_2 * h_2 = \dot{m}_4\,(h_4 - h_5). \tag{30}$$

Throttling valve energetic balance for solution is given as

$$(h_5 \cong h_6). \tag{31}$$

Throttling valve energetic balance for steam is given as

$$(h_8 \cong h_9). \tag{32}$$

The evaporator energetic balance is given as

$$\dot{Q}_{\text{eva}} = \dot{m}_9 * h_9 - \dot{m}_{10} * h_{10} = \dot{m}_{21}\,(h_{21} - h_{22}). \tag{33}$$

The energetic balance for the generator is given as

$$\dot{Q}_{\text{gen}} = \dot{m}_3 * h_3 - \dot{m}_7 * h_7 - \dot{m}_4 * h_4 = \dot{m}_{11}\,(h_{16} - h_{11}). \tag{34}$$

The work done by the pump is given as

$$W_{\text{pump}} = \dot{m}_1 * v_1\,\frac{P_{\text{high}} - P_{\text{low}}}{1000}. \tag{35}$$

The exergy destruction rate of the absorber is given as

$$\begin{aligned}\dot{\mathrm{Ex}}_{\text{ab}} &= \dot{m}_{10} * \mathrm{ex}_{10} + \dot{m}_6 * \mathrm{ex}_6 - \dot{m}_1 * \mathrm{ex}_1 + \dot{m}_{17} * \mathrm{ex}_{17}\\&\quad - \dot{m}_{18} * \mathrm{ex}_{18} - \dot{Q}_{\text{ab}}\left(1 - \frac{T_0}{T_{\text{ab}}}\right).\end{aligned} \tag{36}$$

The heat exchanger is defined as

$$\dot{\mathrm{Ex}}_{\text{HX}} = \dot{m}_2 * \mathrm{ex}_2 - \dot{m}_3 * \mathrm{ex}_3 + \dot{m}_4 * \mathrm{ex}_4 - \dot{m}_5 * \mathrm{ex}_5. \tag{37}$$

The condenser is defined as

$$\dot{\mathrm{Ex}}_{\mathrm{con}} = \dot{m}_7 * \mathrm{ex}_7 - \dot{m}_8 * \mathrm{ex}_8 + \dot{m}_{19} * \mathrm{ex}_{19} - \dot{m}_{20} * \mathrm{ex}_{20} - \dot{Q}_{\mathrm{con}}\left(1 - \frac{T_0}{T_{\mathrm{con}}}\right). \tag{38}$$

Throttling valve exergy is calculated as

$$\dot{\mathrm{Ex}}_{\mathrm{exp}\ 1} = \dot{m}_5\left(\mathrm{ex}_5 - \mathrm{ex}_6\right). \tag{39}$$

Throttling valve exergy steam is calculated as

$$\dot{\mathrm{Ex}}_{\mathrm{exp}\ 2} = \dot{m}_8\left(\mathrm{ex}_8 - \mathrm{ex}_9\right). \tag{40}$$

The evaporator is shown as

$$\dot{\mathrm{Ex}}_{\mathrm{eva}} = \dot{m}_9 * \mathrm{ex}_9 - \dot{m}_{10} * \mathrm{ex}_{10} + \dot{m}_{21} * \mathrm{ex}_{21} - \dot{m}_{22} * \mathrm{ex}_{22} + \dot{Q}_{\mathrm{eva}}\left(1 - \frac{T_0}{T_{\mathrm{eva}}}\right). \tag{41}$$

The exergy destruction for the generator is defined as

$$\dot{\mathrm{Ex}}_{\mathrm{gen}} = \dot{m}_3 * \mathrm{ex}_3 - \dot{m}_7 * \mathrm{ex}_7 - \dot{m}_4 * \mathrm{ex}_4 + \dot{m}_{11} * \mathrm{ex}_{11} - \dot{m}_{16} * \mathrm{ex}_{16} + \dot{Q}_{\mathrm{gen}}\left(1 - \frac{T_0}{T_{\mathrm{gen}}}\right). \tag{42}$$

The pump is calculated as

$$\dot{\mathrm{Ex}}_{\mathrm{pump}} = \dot{m}_1\left(\mathrm{ex}_1 - \mathrm{ex}_2\right) + W_{\mathrm{pump}}. \tag{43}$$

COP of the refrigeration cycle is given as

$$\mathrm{COP} = \frac{\dot{Q}_{\mathrm{eva}}}{\dot{Q}_{\mathrm{gen}} + W_{\mathrm{pump}}}. \tag{44}$$

Exergetic efficiency for the refrigeration cycle is given as

$$\eta_{\mathrm{ex}} = \frac{\dot{Q}_{\mathrm{eva}}\left(1 - \left(T_0/T_{\mathrm{eva}}\right)\right)}{\dot{Q}_{\mathrm{gen}}\left(1 - \left(T_0/T_{\mathrm{gen}}\right)\right) + W_{\mathrm{pump}}}. \tag{45}$$

3.4. Cooling Towers. Energetic balance for the cooling tower is given as

$$\dot{Q}_{\mathrm{ct1}} = \dot{m}_{\mathrm{wat}}\left(h_{19} - h_{20}\right) = \dot{m}_{\mathrm{air}}\left(h_{\mathrm{air},2} - h_{\mathrm{air},1}\right), \tag{46}$$

$$\dot{Q}_{\mathrm{ct2}} = \dot{m}_{\mathrm{wat}}\left(h_{17} - h_{28}\right) = \dot{m}_{\mathrm{air}}\left(h_{\mathrm{air},4} - h_{\mathrm{air},3}\right). \tag{47}$$

By neglecting the pressure difference through the cooling tower $P = P_0$, the air exergy is determined as follows [40]:

$$\mathrm{ex}_{\mathrm{air}} = \left(C_{pa} + \omega C_{pv}\right)\left(T - T_0 - T_0 \ln \frac{T}{T_0}\right) + R\,T_0\left(\left(1 + 1.608\omega\right)\ln\left(\frac{1 + 1.608\omega_0}{1 + 1.608\omega}\right) + 1 + 1.608\omega\ \ln\frac{\omega}{\omega_0}\right). \tag{48}$$

Exergy destruction for the cooling tower is given as

$$\dot{\mathrm{Ex}}_{\mathrm{ct1}} = \dot{m}_{\mathrm{wat}}\left(\mathrm{ex}_{19} - \mathrm{ex}_{20}\right) + \dot{m}_{\mathrm{air}}\left(\mathrm{ex}_{\mathrm{air},1} - \mathrm{ex}_{\mathrm{air},2}\right) - \dot{Q}_{\mathrm{ct}}\left(1 - \frac{T_0}{T_{\mathrm{ct}}}\right), \tag{49}$$

$$\dot{\mathrm{Ex}}_{\mathrm{ct2}} = \dot{m}_{\mathrm{wat}}\left(\mathrm{ex}_{17} - \mathrm{ex}_{18}\right) + \dot{m}_{\mathrm{air}}\left(\mathrm{ex}_{\mathrm{air},3} - \mathrm{ex}_{\mathrm{air},4}\right) - \dot{Q}_{\mathrm{ct}}\left(1 - \frac{T_0}{T_{\mathrm{ct}}}\right). \tag{50}$$

Total irreversibility of ARS the system is obtained as

$$\dot{\mathrm{Ex}}_{\mathrm{total}} = \dot{\mathrm{Ex}}_{\mathrm{eva}} + \dot{\mathrm{Ex}}_{\mathrm{gen}} + \dot{\mathrm{Ex}}_{\mathrm{con}} + \dot{\mathrm{Ex}}_{\mathrm{ab}} + \dot{\mathrm{Ex}}_{\mathrm{HX}} + \dot{\mathrm{Ex}}_{\mathrm{pump}} + \dot{\mathrm{Ex}}_{\mathrm{exp}} + \dot{\mathrm{Ex}}_{\mathrm{ct1}} + \dot{\mathrm{Ex}}_{\mathrm{ct2}}. \tag{51}$$

The ratio between the amount of exergy lost in each component and the system's overall exergy destroyed is known as the irreversibility ratio for each component of a solar-powered absorption cooling system, and it is calculated as follows [41]:

$$\mathrm{IR}_k = \frac{\mathrm{Ex}_k}{\mathrm{Ex}_{\mathrm{total}}}. \tag{52}$$

The exergetic fuel depletion ratio (FDR) of a specific component is determined by the relationship between the rate of irreversible exergy loss in each component and the total exergy input to the system [41].

$$\mathrm{FDR}_k = \frac{\mathrm{Ex}_k}{\mathrm{Ex}_s}, \tag{53}$$

where Ex_s is the overall exergy input to the solar-driven absorption refrigeration system.

4. Results and Discussions

The results of the numerical analyses are presented in this section, which were obtained through a computer code for simulating the cycles developed using Engineering Equation Solver (EES) software for solving the model equations (EES software) and to study the different effects of the operating and design parameters on the integrated system energy and exergy performance. These parameters include, on the one hand, the ambient conditions, such as temperature, humidity, and solar radiation, and, on the other, the ARS design parameters, such as generator, condenser, and absorber temperatures. Thus, the effects of the variation in sun radiation on the ETSC and TES are examined. In addition, the effect of variation in the relative humidity on cooling towers exergetic performance is evaluated.

Table 4: Solar-powered ARS thermodynamic analysis operation data.

Point	Temperature (°C)	h (kJ/kg)	s (kJ/kg K)	m (kg/s)	x (% LiBr)	Ex (kJ/kg)
1	40	94.07	0.2462	30.59	0.5491	25.21
2	40	94.07	0.2462	30.59	0.5491	25.21
3	66.31	148.2	0.4122	30.59	0.5491	29.86
4	95	246.2	0.5027	26.1	0.6435	100.9
5	59.8	182.7	0.3213	26.1	0.6435	91.49
6	59.34	182.7	0.3213	26.1	0.6435	91.49
7	74.3	2639	8.454	4.49		124.2
8	40	167.5	0.5724	4.49		1.464
9	10	167.5	0.5944	4.49		-5.079
10	10	2519	8.9	4.49		-128.4
11	100	227.8	0.7598	787.5		6.659
12	90	210.5	0.7129	649.7		3.278
13	90	210.4	0.7129	649.7		2.429
14	120	262.7	0.8535	649.7		12.9
15	110	245.4	0.8066	787.5		9.516
16	110	245.3	0.8066	787.5		9.407
17	30	125.7	0.4368	631.8		0.08774
18	35	146.6	0.5051	631.8		0.6118
19	30	125.7	0.4368	531		0.08774
20	35	146.6	0.5051	531		0.6118
21	20	83.91	0.2965	504.5		0.0688
22	15	60.45	0.2245	504.5		0.6874

The initial conditions mentioned in Table 1 are utilized to simulate the system. The results of the energetic and exergetic analysis of the reference case are shown in Table 4 for the various state points as pretested in system layout shown in Figure 1.

4.1. Validation of the Model. Before using the model for further analysis and parametric study, the model is validated using some published studies [15]. Table 2 represents the compression of the current model results of the energy rates, COP, and exergetic efficiency compared with that of Modi et al. for a single-effect absorption refrigeration system. The error is very minor and can be attributed to some approximations. However, the results are in agreement with the published data, and the model is considered valid. A cooling tower is added to the cycle instead of the internal heat exchanger to assist the performance. The validation results are listed in Table 5.

Table 5: Model validation table.

Component	Study of [15] (kW)	Present work* (kW)	Relative difference (%)
Generator	4.617	4.651	0.00731
Absorber	4.409	4.472	0.014088
Condenser	3.708	3.699	-0.00243
Evaporator	3.5	3.52	0.005682
SHX	0.9941	0.7989	-0.24434
Pump	0.000075	0.00009059	0.172094
	COP = 0.758	COP = 0.7568	-0.001585
	$\eta_{ex} = 0.24$	$\boldsymbol{\eta}_{\mathbf{ex}} = 0.2329$	0.02958

* Input parameters for validation: $T_{cond} = T_{abs} = 40°C$, $T_{gen} = 87°C$, $Q_{eva} = 1$ TR.

4.2. Evacuated Tube Solar Collector. The variation of exergy and energy is present for the ETSC with different parameters, such as sun radiation on typical summer and winter days, i.e., 23 June and 11 December 2002 for Al-Madinah City in Saudi Arabia. Figure 5 shows the variations in the mass flow produced by the solar collector in kilograms per hour over time in summer and winter. According to this figure, the mass flow increases with the increase of solar radiation, where it peaks at 13 : 00 in summer and 12 : 00 in winter, and then decreases with sunset. When there is no radiation, the collector ceases to supply the mass flow in both seasons, and the ARS must utilize the thermal energy stored in the TES.

In Figure 6, the exergetic and energetic efficiencies of the solar collector are observed to follow the sun's radiation over the daytime, in summer, and in winter. In summer, the maximum energetic and exergetic efficiencies are achieved at about 13 : 00 with a value of 48% and 10%, respectively, when the sun radiation value peaks, then decreases slightly till 18 : 00, and rapidly drops due to the diminishing sun radiation. In winter, the maximum sun radiation is detected at 12 : 00; at that hour, the energetic and exergetic

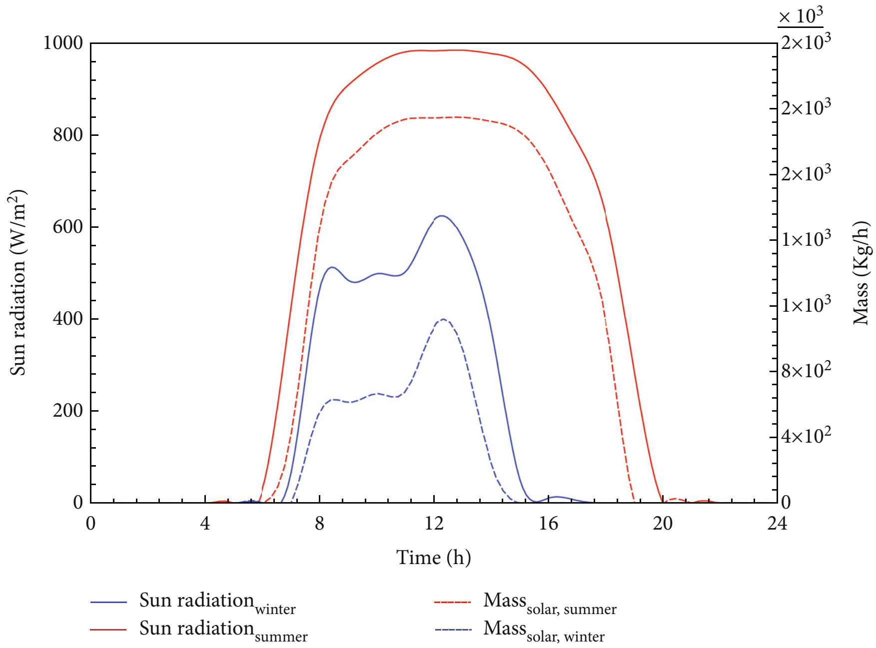

FIGURE 5: Effect of sun radiation on the mass produced from the solar collector over time during typical summer and winter days.

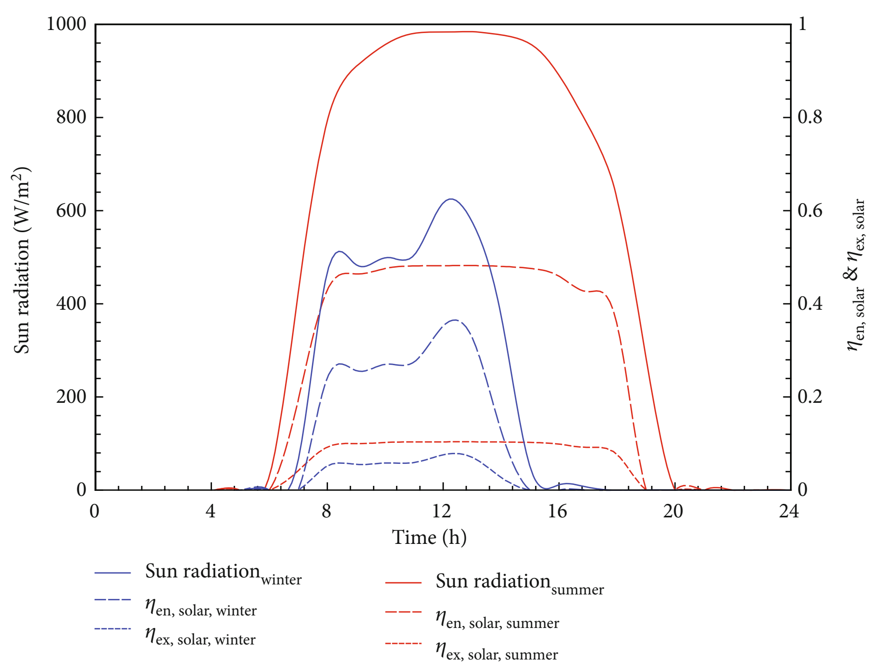

FIGURE 6: Effect of sun radiation on the energetic and exergetic efficiencies of the ETSC over time on typical summer and winter days.

efficiencies peak recording 35% and 7%, respectively. The energy and exergy efficiencies of the solar collector are higher for the summer season compared with the winter season, and the reason for that is the reduced ambient temperature during the winter season which causes larger heat losses from the solar collector as shown in equation (8). A similar result was reported for ETSC efficiency by Eltaweel et al. [34], where they studied the effect of multi-walled nanotubes and water nanofluid as a working fluid on the energetic and exergetic efficiencies of the evacuated tube solar collectors.

Figure 7 shows the magnitude of the useful solar energy and associated exergy destruction that can be produced using ETSC with different areas based on the location provided in Table 1. The figure also shows how the collector area plays a significant role in achieving the energy needed for thermal storage to power the ARS considering the additional energy needed for continuous operation and to

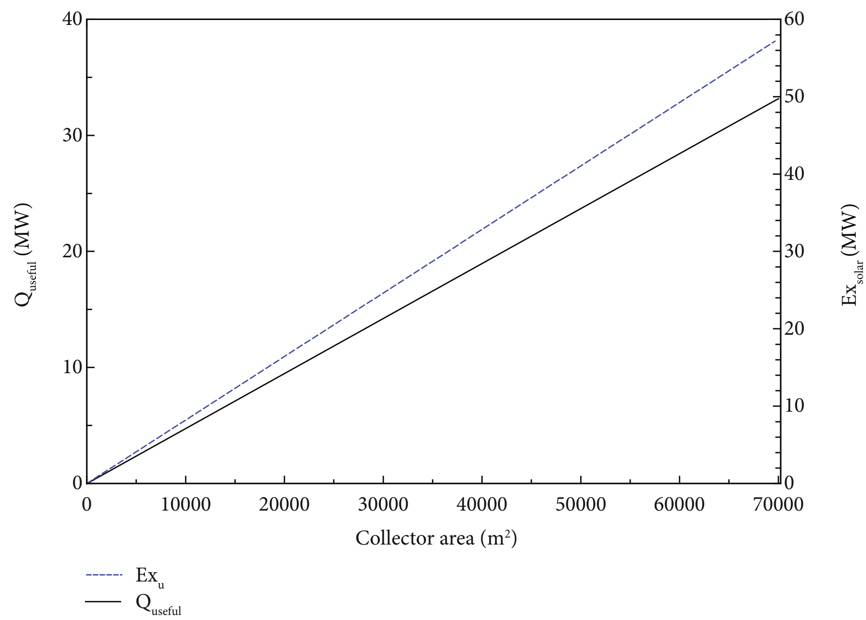

Figure 7: Effect of the collector area on solar useful energy and exergy destruction of the collector.

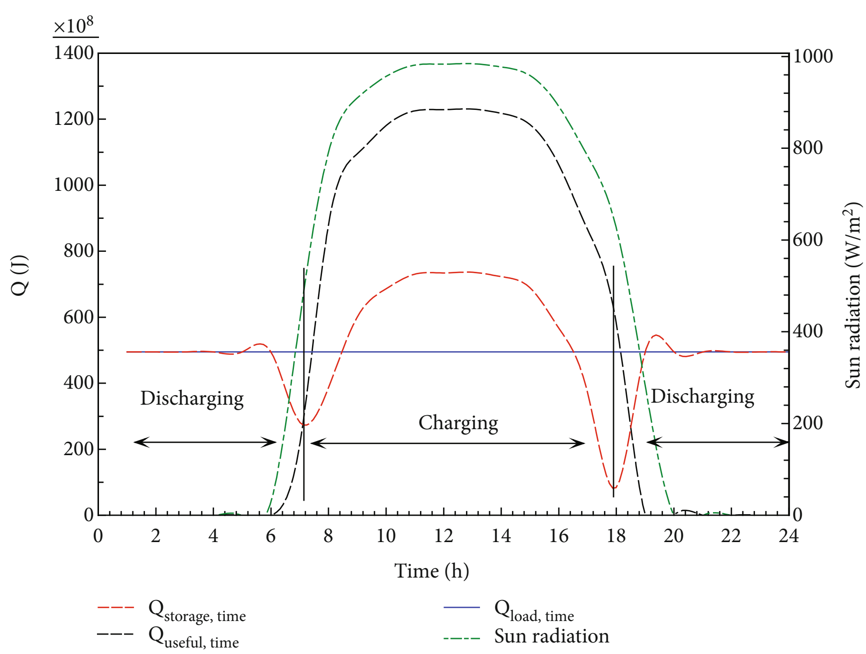

Figure 8: Variation of useful solar energy over time alongside the energy needed for the system of 3 kTR and TES energy stored for summer.

overcome heat losses. The collector area required to achieve the cooling load of 3000 TR for the ARS for 24 h is evaluated at 72060 m^2. It must be mentioned that the variation between solar collector production in summer and winter is significant as radiation availability significantly varies; however, for the cooling systems, the design is typically done for summer, which advantageously coincides with high solar radiation. On the other hand, during winter, the cooling loads reduce considerably, and the low radiation may be just enough. In addition, these results are related to the location considered in this study, for example, another location with higher or lower solar radiation, and cooling load is expected to have a different set of design requirements, i.e., collector area and thermal energy storage.

4.3. TES. Analyze the TES energy and exergy to ensure the proper energy supply for the ARS and how the different parameters affect the TES. Figure 8 describes the effect of sun radiation on the solar useful heat gain over the variation of time with the cooling load of the ARS and the energy

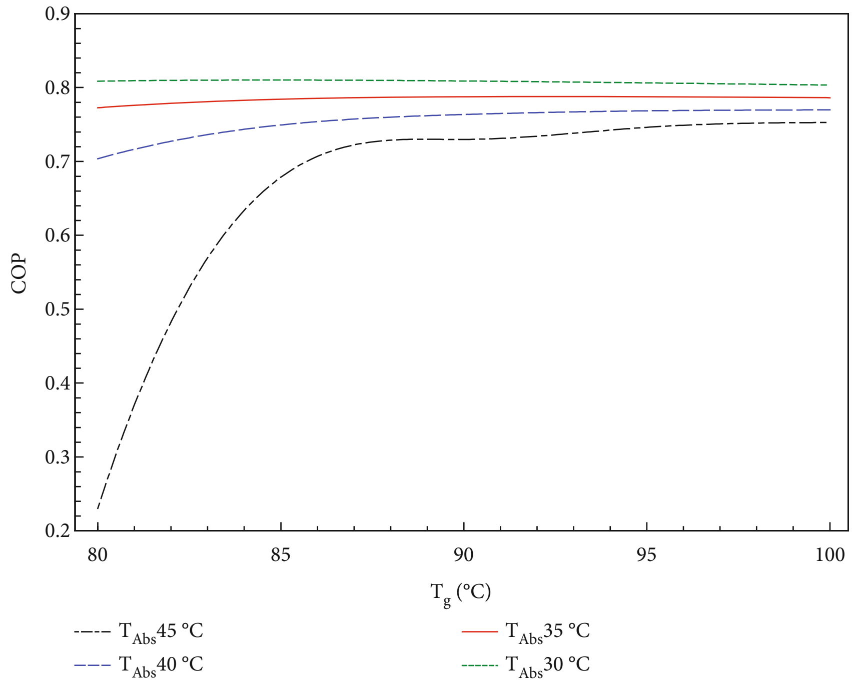

FIGURE 9: Effect of generator temperature on COP and absorber temperature at $T_{eva} = 10^{\circ}C$, $T_{cond} = 40^{\circ}C$, and $Q_{eva} = 3\,kTR$.

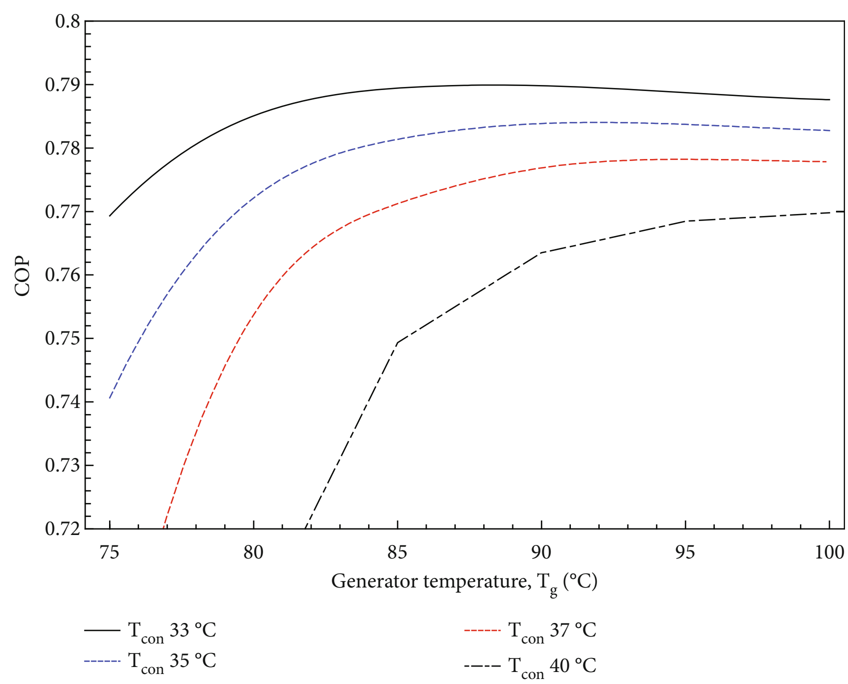

FIGURE 10: Effect of generator temperature on COP and condenser temperature at $T_{eva} = 10^{\circ}C$.

stored in the TES. It shows that solar useful heat gain increases with increasing the sun radiation from 7 : 00, the maximum value reached at 13 : 00, after which it begins to decrease till it reaches 18 : 00 when there is little to no solar radiation. The red line represents the magnitude of the energy flowing to and from the TES according to the charging and discharging processes. For example, the thermal storage tank discharges the heat during nighttime to power the ARS, and with the sunrise (between 6 : 00 and 8 : 00), the heat discharging reduces to stop and converts to charging when the mass flow rate coming from the solar collector is more than that needed for operating the ARS. It can be observed that the TES receives maximum flow rate at maximum radiation, and the charging process for a typical

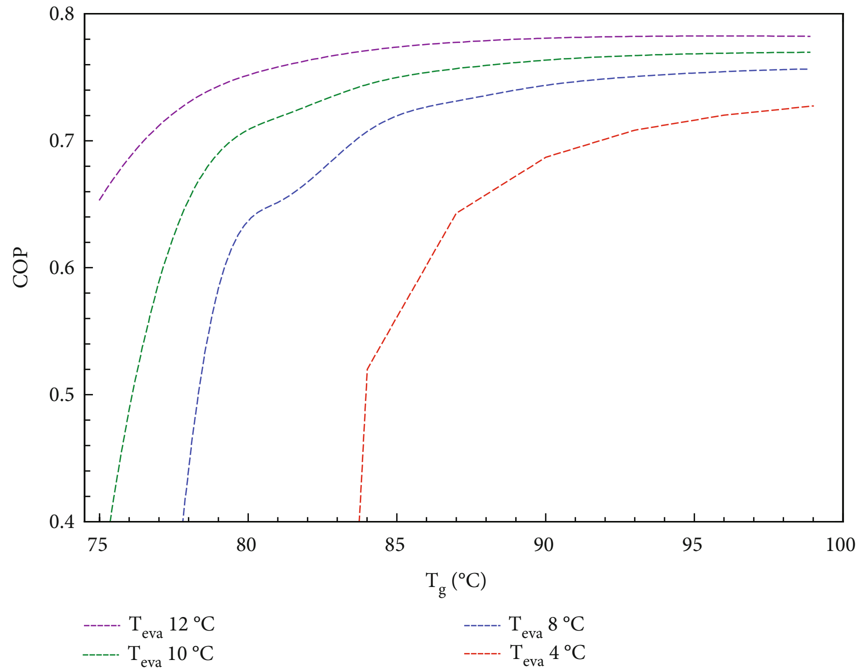

Figure 11: Effect of generator temperature on COP and evaporator temperature at $Q_{eva} = 3$ TR and $T_{con} = 40^{\circ}$C.

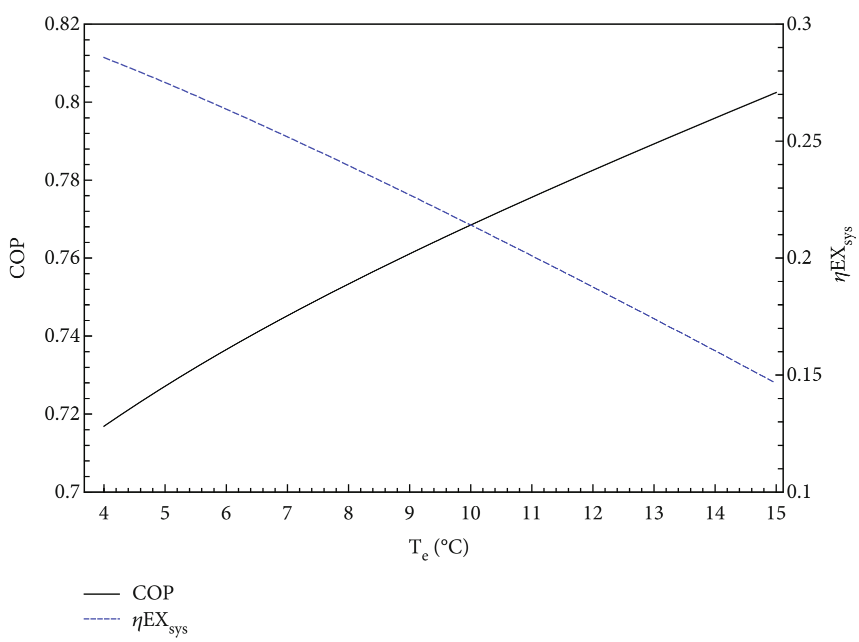

Figure 12: Effect of evaporator temperature on COP and exergetic efficiency at $T_{gen} = 95^{\circ}$C.

summer day starts at about 7 : 00 unit 18 : 00; after that, it operates in discharging mode. It is determined that a tank volume of 43292 m^3 is required to meet the desired cooling load (evaporator capacity) of 3000 TR of the ARS so that the system can operate for a whole day. The TES energetic and exergetic efficiencies for the day selected for the analysis are 99% and 98%, respectively. These figures are typical for TES with high insulation.

4.4. ARS. Different key parameters are defined to analyze the energy and exergy performance of the ARS, such as generator, condenser, absorber, and evaporator temperatures. All the parameters that may affect the system's performance are considered. For instance, a summer representative day is selected, i.e., 23 June 2002 for Al-Madinah City in Saudi Arabia. Table 1 shows the values of the parameters used in the analysis. Figure 9 shows the effects of changing the

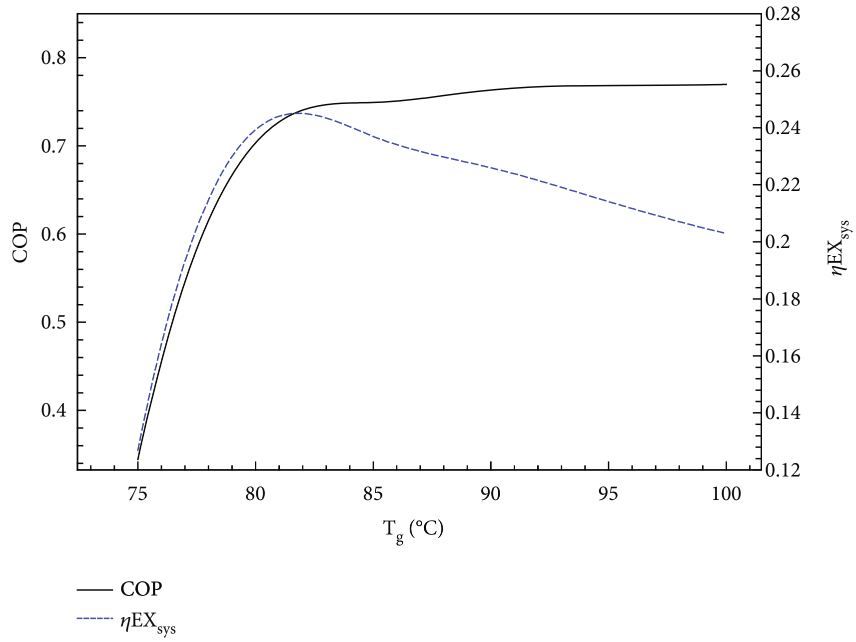

Figure 13: Effect of generator temperature on COP and exergetic efficiency at $T_{eva} = 10^{\circ}C$ and $Q_{eva} = 3\,kTR$.

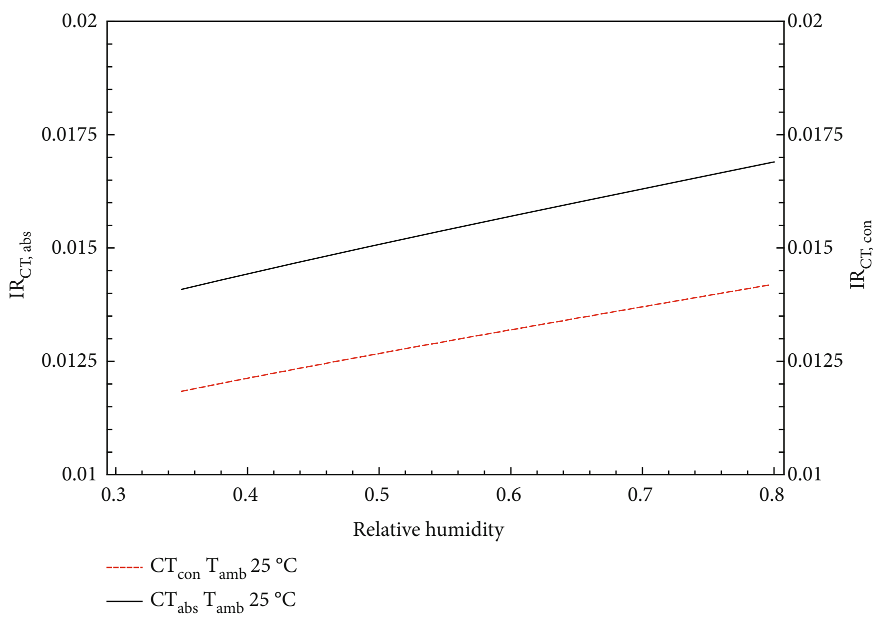

Figure 14: Effect of relative humidity on cooling towers' irreversibility rates.

generator temperature on the COP of the ARS for different absorber operating temperatures. The COP shows a slight increase with increasing the operating temperature of the generator. However, at higher absorber temperatures, e.g., 45°C, the COP considerably reduces when the generator temperature drops below 88°C.

Figure 10 describes the change in the COP due to the variation in the generator operating temperature with the change in condenser temperatures. As shown, the COP increases with the increase of the generator temperature till it reaches a specific temperature, and then, the COP shows less change. Also, it shows how decreasing the absorber temperature affects the COP positively. As for the condenser temperature, by observing Figure 11, it can be indicated that it has a similar effect on the COP as the absorber when lowering its temperature. The best COP result in the analysis occurs at 33°C and 30°C of the condenser and absorber temperature, respectively.

In Figure 12, the effect of increasing the evaporator temperature on the COP and the system exergetic efficiency is

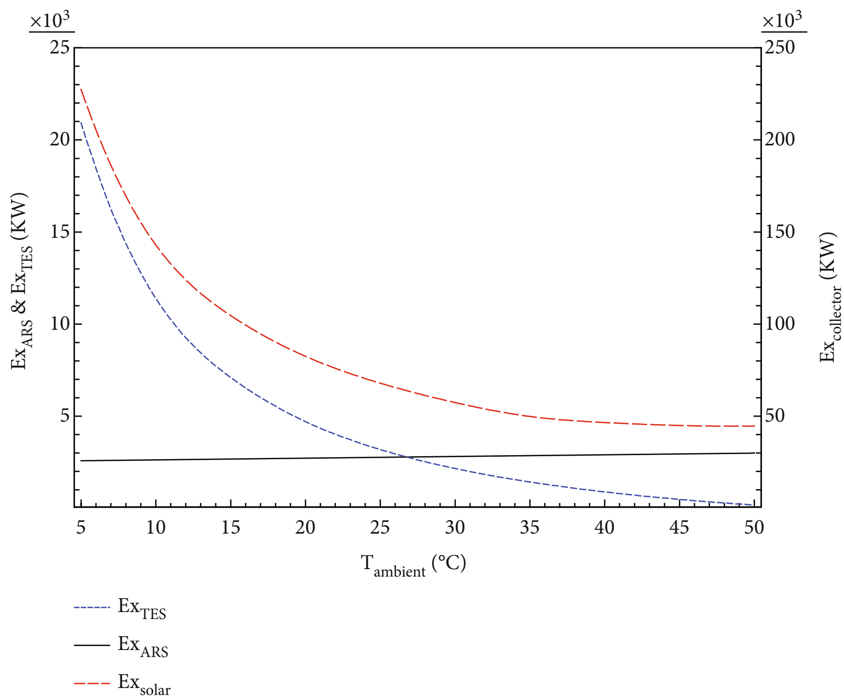

Figure 15: Effect of ambient temperature on the collector, TES, and ARS.

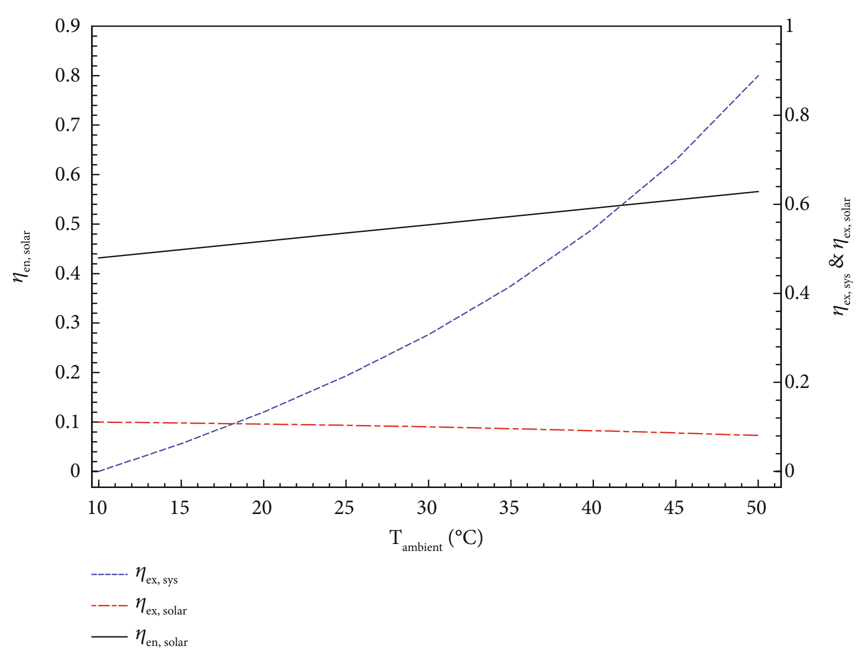

Figure 16: Effect of ambient temperature on the collector efficiency and exergetic efficiency of the collector and the ARS.

reported. The COP increases with the increase in the evaporator temperature, while the exergetic efficiency has an opposite trend. The COP shows a linear increase, achieving 0.782 at 12°C. However, the exergetic efficiency decreases varying between 15% and 28%. These results for both COP and exergetic efficiency are consistent with literature, for example, the exergetic efficiency reported to be 14.5% at 15°C [15]. Moreover, Kaushik and Arora [13] observed the same behavior of the exergetic efficiency with respect to evaporator temperature.

The same effect analysis has been defined in Figure 13 with the variation of generator temperature where the highest value for exergetic efficiency 24% occurs at 82°C and then decreases due to the increase in the generator exergy loss. Also, it can be observed that the COP increases with the increase of the generator temperature. Figure 13 provides a

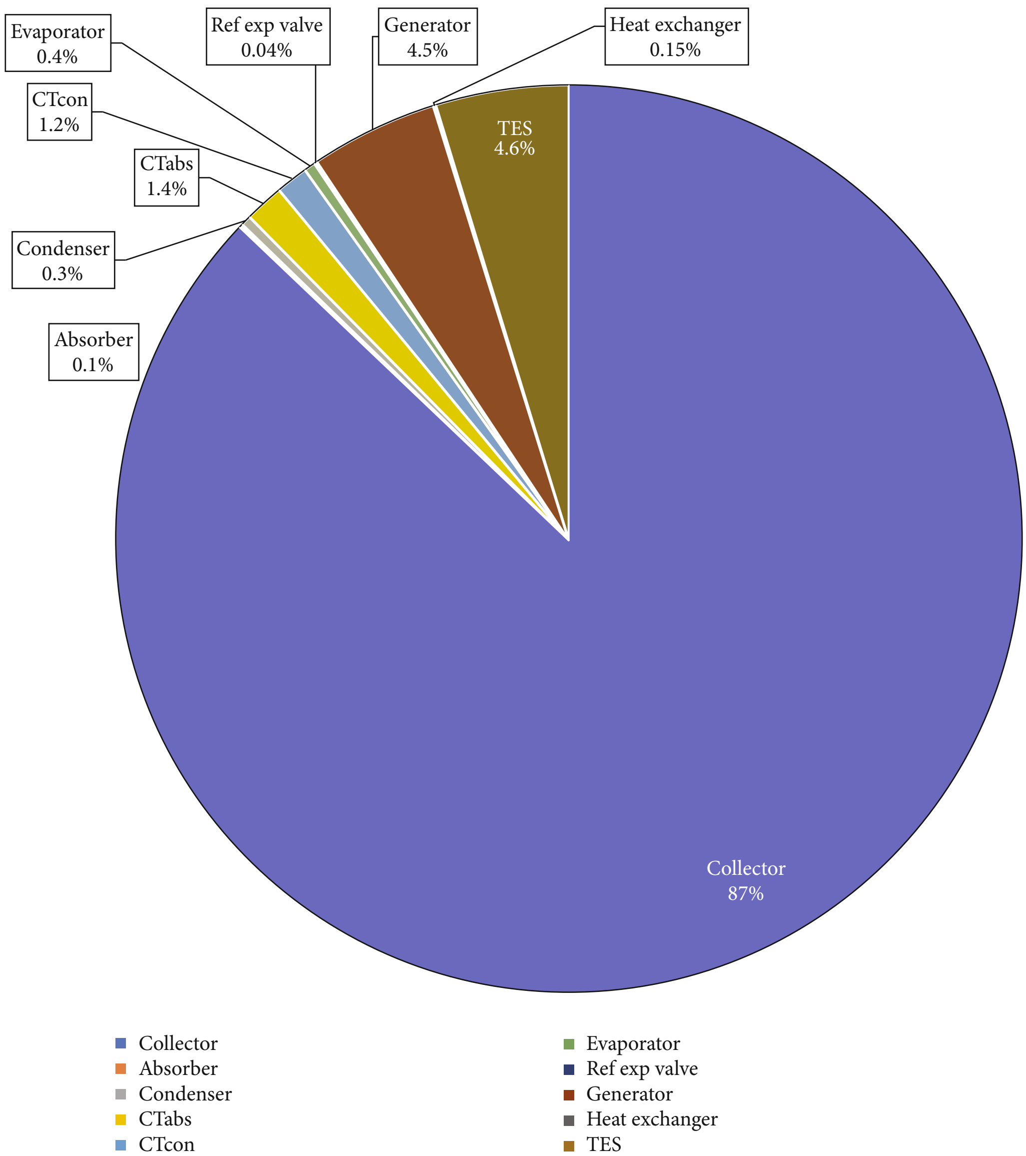

Figure 17: Distribution irreversibility rate between solar-driven ARS components.

useful mean of the system optimization, where a maximum exergetic performance point is obtained, i.e., generator temperature of 82°C. Therefore, this finding suggests that for the specified location and cooling load considering the proposed system, the optimum temperature for operating the generator is 82°C, and increasing generator temperature, though it slightly increases the COP, will lead to more exergy destruction that causes the overall system exergetic efficiency to decline. This finding also emphasizes the advantage of conducting an exergy analysis as compared to an energy analysis.

4.5. Cooling Towers. Figure 14 describes the effect of the cooling towers' irreversibility rate due to the relative humidity variation. This figure shows that the irreversibility rates increase with the increase in the relative humidity, where the higher irreversibility rate values of 0.017 and 0.0143 occurred at 0.8 relative humidity for both the absorber and the condenser cooling tower, respectively. It is well known that cooling towers operate more effectively at reduced relative humidity. Thus, higher specific humidity can be achieved leading to higher evaporative cooling, the operating principle of cooling tower. However, when the ambient relative humidity increases, lower evaporative cooling can be achieved; thus, cooling towers are less effective. The impact of this on the overall system can be observed in the increased operating temperature of the condenser and absorber, which is reflected in reduced overall system COP, as already observed in Figures 9 and 10.

4.6. Overall System Performance. The effect of the ambient temperature on the exergy loss within the collector, TES, and ARS can be observed in Figure 15. It is shown that the ARS exergy increases with the increase of the ambient temperature, whereas the solar collector exergy decreases with a higher ambient temperature. The same occurs for the total

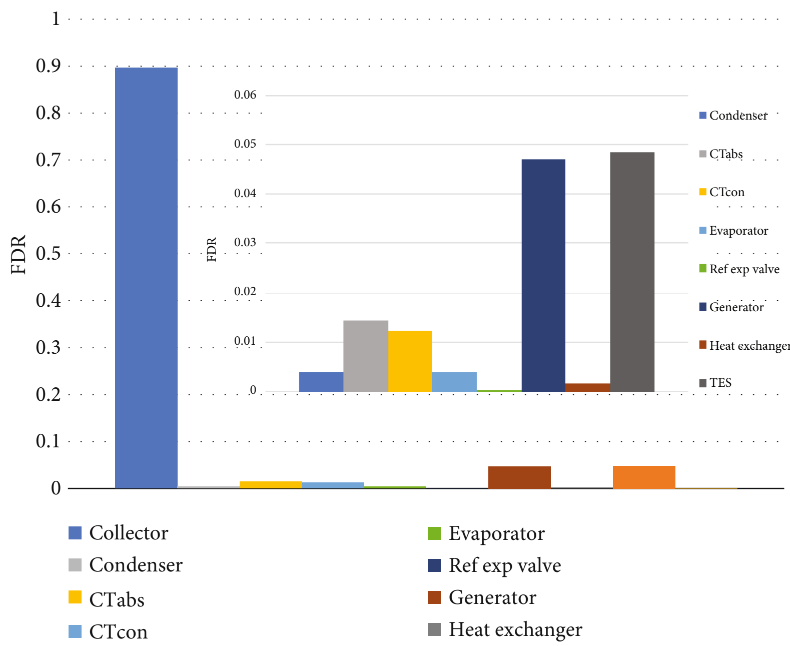

Figure 18: Variation of FDR value of solar-driven ARS components.

Table 6: Various solar thermal collectors coupled with vapor absorption chillers [18].

Solar thermal collectors	Collector area (m^2)	Cooling capacity (kW)	TES tank size (m^3)	COP	Reference
Flat plate collectors	56	12.31	24	—	Sayigh and Khoshaim [45]
Evacuated tube collector	12	4.5	—	0.58	Agyenim et al. [46]
Evacuated tube collector	108	35.17	—	0.37–0.81	Ali et al. [47]
Flat plate collectors	36	4	0.3 (HW) + 2 (CW)	0.54	Van Hattem and Actis Data [48]
Evacuated tube collectors	1577 nos.	211.02	15	0.618	Al-Karaghouli et al. [49]
Flat plate collectors	38.2	4.7	2.75		Yeung et al. [50]
Flat plate collectors	113	35.17	5.7	0.63	Meza et al. [51]
Flat plate collectors	316	90	30	053–0.73	Best and Ortega [52]
Flat plate collectors	38	4.7	2.75	0.07 (COP overall)	Li and Sumathy [53]
Flat plate collectors	49.9	35.17	2	0.42	Syed et al. [54]
Flat plate collectors	151	35.17	2.5	0.41–0.66	Zambrano et al. [55]
Evacuated tube collectors	72	35.17	0.4	0.7	Pongtornkulpanich et al. [24]
Evacuated tube collectors	72060	10,560	43292	0.77	Current study

HW: hot water; CW: cold water.

exergy destruction within the TES. The highest values of exergy destruction that the solar collector, TES, and ARS experienced at maximum ambient temperature (at 50°C) are 44652 KW, 172.2 KW, and 2996 KW, respectively.

The effect of the ambient temperature on the energetic and exergetic efficiency of the collector and the ARS can be observed in Figure 16, where the energy efficiency of the solar collector increases within the rising ambient temperature. The exergy efficiency of the ARS also increases alongside the increase in the ambient temperature due to the exergy of heat. However, the collector exergy efficiency shows a slight decrease; the collector exergy efficiency obtained at 25°C is 10%, while the ARS exergy efficiency is 21%. This figure shows that though the energy efficiency of the collector appears to increase with ambient temperature due to reduced energy losses, the exergy analysis is less sensitive to these losses as they are low-grade heat, and its exergetic quality reduces with the increase in the ambient temperature. Thus, the advantage of conducting exergy analysis in addition to energy analysis can be realized, and the focus of the designer and system optimizer can be directed to losses that impact exergetic performance.

Figure 17 shows the irreversibilities (exergy destruction rates) of the system component and their distribution among the system components. It can be clearly observed that the solar collector consumes the largest share of 87% of the total exergy destruction of the system. Thus, this finding indicates, on one hand, that the collector deserves more research and development for improving exergetic performance, while on the other, it shows that the nature of solar energy capture involves significant exergy destruction. The TES exergy destruction came second with only 4.6% of the total exergy destruction. Finally, the generator destroyed about 4.5%. Here, the generator deserves some effort to reduce the exergy destruction rate which can be achieved by enhancing the heat transfer process within the generator and optimizing the generator heat exchanger for better heat utilization.

Figure 18 describes the distribution of the FDR between the system components. It illustrates that the solar collector depletes 89% of the input exergy; 4.8% goes for TES where the generator depletes 4.7%. These figures compare the performance of the various components to direct the researchers and technology developers to the ones that deserves more attention and can have potential for improvement.

Table 6 represents the compression of the current model with various LiBr-H_2O absorption chillers coupled with solar thermal collectors working in different collector areas, tank volumes, and cooling capacities. It must be emphasized that Table 6 included some systems that use flat plate collectors while some used evaluated tube collectors; this will clearly show the contribution of the current study and benchmark the performance of the current system compared with those studied in the literature.

5. Conclusion

In this study, an energy and exergy analysis is conducted on a solar-powered LiBr-H_2O ARS. An evacuated solar collector is used in integration with TES to continuously provide the required heat for the ARS, while cooling towers are used to provide the cooling required for the condenser and the absorber. The proposed system is modeled and solved for two cases, one for the summer and another for the winter. The results of this study can be summarized in the following points:

(i) The increase of the sun radiation causes an increase in solar field mass, collector useful heat, and energy stored in the TES, where energy stored reaches its peak at 1 p.m. It also increases the energetic and exergetic efficiencies of the solar collector

(ii) Lowering both temperatures of the condenser and absorber positively impacts the COP of the ARS; however, it increases with the decrease in their temperatures

(iii) Increasing evaporator temperature resulted in higher COP values of the ARS

(iv) The COP increases with the increase in the generator temperature, while the exergetic efficiency peaks at 82°C achieving a value of 24% and then decreases

(v) The irreversibility rates within the cooling towers show a linear increase with the relative humidity

(vi) The exergy destruction of the ETSC increases with the ambient temperature rising, while the TES and ARS exergy destruction rates decrease. However, the overall system exergetic efficiency is positively affected by the rise in ambient temperature

(vii) The solar collector contributes 87% of the total exergy destruction of the system, 4.6% attributed to the storage tank and 4.5% in the generator

(viii) The collector area required to achieve the cooling load of 3000 TR for the ARS for 24 h is 72060 m^2

As the current study is limited to the single-effect ARS, it is recommended in future work to consider using multieffect ARS to enhance the performance of the integrated cooling system. Also, it is worth examining other solar collector technologies, such as parabolic trough collectors with single- and multieffect ARS. The variation of TES size is another critical parameter that must be examined and optimized in more detailed and dedicated studies.

Nomenclature

Abbreviations

A_c: Area of the collector
C_{pa}: Specific heat of dry air at constant pressure (kJ/kg K)
COP: Coefficient of performance
E: Exergy destruction
ex: Exergy destruction (kW)
F_R: Heat removal factor
h: Enthalpy (kJ/kg)
I: Total solar radiation (W/m^2)
$\dot{m}$: Mass flow rate (kg/s)
m_w: Mass flow rate of water (kg/s)
$\dot{Q}$: Heat transfer rate (kW)
Q_{loss}: Energy loss to the ambient surroundings (kW)
$\dot{Q}_u$: Useful heat gained by the collector (kW)
R: Gas constant (kJ/kg K)
s: Entropy (kJ/kg K)
T: Temperature (°C)

T_{avg}: Average thermal storage temperature (°C)
T_0: Ambient temperature (°C)
T_s: Solar surface temperature (°C)
U_l: Overall heat transfer coefficient
v: Specific volume (m^3/kg)
W: Work (kW).

Greek Symbols

ω: Humidity ratio (kgw/kga)
η_{ex}: Exergetic efficiency of absorption system
η_{TES}: Energetic efficiency of thermal storage
α: Absorptivity
η_c: Efficiency of the collector
η_{ex-TES}: Exergetic efficiency of absorption system
$\boldsymbol{\tau}$: Transmissivity.

Subscripts

exp: Expansion valve
0: Dead state
ct: Cooling tower
eva: Evaporator
ref: Refrigerant
con: Condenser
ab: Absorber
gen: Generator
in: Input
out: Output
HX: Solution heat exchanger
TES: Thermal energy storage.

Data Availability

All data used are included in the manuscript.

Conflicts of Interest

The authors reported no conflict of interest.

Acknowledgments

The authors extend their appreciation to the Deanship for Research & Innovation, Ministry of Education in Saudi Arabia, for funding this research work through the project number IFP22UQU4310024DSR199.

References

[1] N. Khan, M. Khan, M. Ashar, and A. Z. Khan, "Energy and exergy analysis of vapour compression refrigeration system with R12, R22, R134a," *International Journal of Emerging Technology and Advanced Engineering*, vol. 5, no. 3, pp. 210–216, 2015.

[2] B. S. Bagheri, R. Shirmohammadi, S. M. S. Mahmoudi, and M. A. Rosen, "Optimization and comprehensive exergy-based analyses of a parallel flow double-effect water-lithium bromide absorption refrigeration system," *Applied Thermal Engineering*, vol. 152, pp. 643–653, 2019.

[3] S. Gong and K. G. Boulama, "Parametric study of an absorption refrigeration machine using advanced exergy analysis," *Energy*, vol. 76, pp. 453–467, 2014.

[4] M. S. Mazzei, M. C. Mussati, and S. F. Mussati, "NLP model-based optimal design of LiBr–H2O absorption refrigeration systems," *International Journal of Refrigeration*, vol. 38, pp. 58–70, 2014.

[5] C. Babu and P. Ponnambalam, "The role of thermoelectric generators in the hybrid PV/T systems: a review," *Energy Conversion and Management*, vol. 151, pp. 368–385, 2017.

[6] M. Eltaweel, A. A. Abdel-Rehim, and H. Hussien, "Indirect thermosiphon flat-plate solar collector performance based on twisted tube design heat exchanger filled with nanofluid," *International Journal of Energy Research*, vol. 44, no. 6, p. 4278, 2020.

[7] R. Tang, Z. Li, H. Zhong, and Q. Lan, "Assessment of uncertainty in mean heat loss coefficient of all glass evacuated solar collector tube testing," *Energy Conversion and Management*, vol. 47, no. 1, pp. 60–67, 2006.

[8] A. A. AlZahrani, *Development and Analysis of a Solar-Based Integrated System with a CO_2 Rankine Power Cycle*, Masters, University of Ontario Institute of Technology, Ontario, Canada, 2013.

[9] R. Gomri, "Second law comparison of single effect and double effect vapour absorption refrigeration systems," *Energy Conversion and Management*, vol. 50, no. 5, pp. 1279–1287, 2009.

[10] R. D. Misra, P. K. Sahoo, S. Sahoo, and A. Gupta, "Thermoeconomic optimization of a single effect water/LiBr vapour absorption refrigeration system," *International Journal of Refrigeration*, vol. 26, no. 2, pp. 158–169, 2003.

[11] A. Şencan, K. A. Yakut, and S. A. Kalogirou, "Exergy analysis of lithium bromide/water absorption systems," *Renewable Energy*, vol. 30, no. 5, pp. 645–657, 2005.

[12] O. Kaynakli and M. Kilic, "Theoretical study on the effect of operating conditions on performance of absorption refrigeration system," *Energy Conversion and Management*, vol. 48, no. 2, pp. 599–607, 2007.

[13] S. C. Kaushik and A. Arora, "Energy and exergy analysis of single effect and series flow double effect water-lithium bromide absorption refrigeration systems," *International Journal of Refrigeration*, vol. 32, no. 6, pp. 1247–1258, 2009.

[14] W. Rivera, J. Cerezo, and H. Martínez, "Energy and exergy analysis of an experimental single-stage heat transformer operating with the water/lithium bromide mixture," *International Journal of Energy Research*, vol. 34, no. 13, p. 1131, 2010.

[15] B. Modi, A. Mudgal, and B. Patel, "Energy and exergy investigation of small capacity single effect lithium bromide absorption refrigeration system," *Energy Procedia*, vol. 109, pp. 203–210, 2017.

[16] O. Kaynakli, K. Saka, and F. Kaynakli, "Energy and exergy analysis of a double effect absorption refrigeration system based on different heat sources," *Energy Conversion and Management*, vol. 106, pp. 21–30, 2015.

[17] S. Mohtaram, M. Omidi, J. Lin, H. Sun, and W. Chen, "Exergy analysis of a multi mixture working fluid absorption refrigeration cycle," *Case Studies in Thermal Engineering*, vol. 15, article 100540, 2019.

[18] T. Ahmad, M. Azhar, M. K. Sinha, M. Meraj, I. M. Mahbubul, and A. Ahmad, "Energy analysis of lithium bromide-water and lithium chloride-water based single effect vapour absorption

refrigeration system: a comparison study," *Cleaner Engineering and Technology*, vol. 7, article 100432, 2022.

[19] A. A. AlZahrani and I. Dincer, "Energy and exergy analyses of a parabolic trough solar power plant using carbon dioxide power cycle," *Energy Conversion and Management*, vol. 158, pp. 476–488, 2018.

[20] A. A. R. AlZahrani and I. Dincer, *Rankine Cycle Power Generation System with Sc-Co2 Working Fluid and Integrated Absorption Refrigeration Chiller*, U.S. Patent Application 14/514,488, 2014.

[21] G. Leonzio, "Solar systems integrated with absorption heat pumps and thermal energy storages: state of art," *Renewable and Sustainable Energy Reviews*, vol. 70, pp. 492–505, 2017.

[22] A. Ileri, "Yearly simulation of a solar-aided R22-DEGDME absorption heat pump system," *Solar Energy*, vol. 55, no. 4, pp. 255–265, 1995.

[23] B. Rezaie, B. V. Reddy, and M. A. Rosen, "Exergy analysis of thermal energy storage in a district energy application," *Renewable Energy*, vol. 74, pp. 848–854, 2015.

[24] A. Pongtornkulpanich, S. Thepa, M. Amornkitbamrung, and C. Butcher, "Experience with fully operational solar-driven 10-ton LiBr/H_2O single-effect absorption cooling system in Thailand," *Renewable Energy*, vol. 33, no. 5, pp. 943–949, 2008.

[25] C. Onan, D. B. Ozkan, and S. Erdem, "Exergy analysis of a solar assisted absorption cooling system on an hourly basis in villa applications," *Energy*, vol. 35, no. 12, pp. 5277–5285, 2010.

[26] K. Sumathy, Z. C. Huang, and Z. F. Li, "Solar absorption cooling with low grade heat source - a strategy of development in South China," *Solar Energy*, vol. 72, no. 2, pp. 155–165, 2002.

[27] E. D. Kerme, A. Chafidz, O. P. Agboola, J. Orfi, A. H. Fakeeha, and A. S. Al-Fatesh, "Energetic and exergetic analysis of solar-powered lithium bromide-water absorption cooling system," *Journal of Cleaner Production*, vol. 151, pp. 60–73, 2017.

[28] S. Rosiek, "Exergy analysis of a solar-assisted air-conditioning system: case study in southern Spain," *Applied Thermal Engineering*, vol. 148, pp. 806–816, 2019.

[29] E. Bellos and C. Tzivanidis, "Thermal analysis of parabolic trough collector operating with mono and hybrid nanofluids," *Sustainable Energy Technologies and Assessments*, vol. 26, pp. 105–115, 2018.

[30] A. Nasr, "Thermal protection of a vertical plate using ethylene glycol film cooling flowing down on a vertical plate," *Journal of Umm Al-Qura University for Engineering and Architecture*, vol. 14, no. 2, pp. 135–141, 2023.

[31] S. A. Kalogirou, "Solar thermal collectors and applications," *Progress in Energy and Combustion Science*, vol. 30, no. 3, pp. 231–295, 2004.

[32] R. Hirmiz, M. F. Lightstone, and J. S. Cotton, "Performance enhancement of solar absorption cooling systems using thermal energy storage with phase change materials," *Applied Energy*, vol. 223, pp. 11–29, 2018.

[33] Y. A. Çengel and M. A. Boles, *Thermodynamics: an engineering approach*, McGraw-Hill Education, 2002.

[34] M. Eltaweel, A. A. Abdel-Rehim, and A. A. A. Attia, "Energetic and exergetic analysis of a heat pipe evacuated tube solar collector using MWCNT/water nanofluid," *Case Studies in Thermal Engineering*, vol. 22, article 100743, 2020.

[35] S. A. Kalogirou, S. Karellas, K. Braimakis, C. Stanciu, and V. Badescu, "Exergy analysis of solar thermal collectors and processes," *Progress in Energy and Combustion Science*, vol. 56, pp. 106–137, 2016.

[36] J. A. Duffie and W. A. Beckman, *Solar Engineering of Thermal Processes: Fourth Edition*, Wiley, 2013.

[37] İ. Dinçer and M. A. Rosen, *Thermal Energy Storage*, Wiley, 2010.

[38] A. A. AlZahrani and I. Dincer, "Comparative energy and exergy studies of combined CO_2 Brayton-organic Rankine cycle integrated with solar tower plant," *International Journal of Exergy*, vol. 26, no. 1-2, pp. 21–40, 2018.

[39] A. A. AlZahrani and I. Dincer, "Performance assessment of an aquifer thermal energy storage system for heating and cooling applications," *Journal of Energy Resources Technology*, vol. 138, no. 1, article 011901, 2016.

[40] T. Muangnoi, W. Asvapoositkul, and S. Wongwises, "An exergy analysis on the performance of a counterflow wet cooling tower," *Applied Thermal Engineering*, vol. 27, no. 5–6, pp. 910–917, 2007.

[41] A. Bejan, G. Tsatsaronis, and M. Moran, *Thermal Design and Optimization*, Wiley-Interscience, 1995.

[42] K. E. Herold, R. Radermacher, and S. A. Klein, *Absorption Chillers and Heat Pumps*, CRC Press, 2016.

[43] S. M. A. Aljeddani, "Forecasting temperature of the Saudi Arabian Province of Makkah using a discrete state–space modeling approach," *Journal of Umm Al-Qura University for Engineering and Architecture*, vol. 14, no. 2, pp. 79–94, 2023.

[44] NERL, "nrel.gov/grid/solar-resource/saudi-arabia," https://www.nrel.gov/grid/solar-resource/saudi-arabia.html.

[45] A. A. M. Sayigh and B. H. Khoshaim, "A three and a half ton solar absorption air conditioner's performance in Riyadh, Saudi Arabia," *Solar Cooling and Dehumidifying*, vol. 1, p. 49, 1981.

[46] F. Agyenim, I. Knight, and M. Rhodes, "Design and experimental testing of the performance of an outdoor LiBr/H2O solar thermal absorption cooling system with a cold store," *Solar Energy*, vol. 84, no. 5, pp. 735–744, 2010.

[47] A. H. H. Ali, P. Noeres, and C. Pollerberg, "Performance assessment of an integrated free cooling and solar powered single-effect lithium bromide-water absorption chiller," *Solar Energy*, vol. 82, no. 11, pp. 1021–1030, 2008.

[48] D. Van Hattem and P. Actis Data, "Description and performance of an active solar cooling system, using a LiBr-H_2O absorption machine," *Energy and Buildings*, vol. 3, no. 2, pp. 169–196, 1981.

[49] A. Al-Karaghouli, I. Abood, and N. I. Al-Hamdani, "The solar energy research center building thermal performance evaluation during the summer season," *Energy Conversion and Management*, vol. 32, no. 5, pp. 409–417, 1991.

[50] M. R. Yeung, P. K. Yuen, A. Dunn, and L. S. Cornish, "Performance of a solar-powered air conditioning system in Hong Kong," *Solar Energy*, vol. 48, no. 5, pp. 309–319, 1992.

[51] J. I. Meza, A. Y. Khan, and J. E. Gonzalez, *Experimental Assessment of a Solar-Assisted Air Conditioning System for Application in Puerto Rico*, Solar Engineering, 1998.

[52] R. Best and N. Ortega, "Solar refrigeration and cooling," *Renewable Energy*, vol. 16, no. 1–4, pp. 685–690, 1999.

[53] Z. F. Li and K. Sumathy, "Experimental studies on a solar powered air conditioning system with partitioned hot water storage tank," *Solar Energy*, vol. 71, no. 5, pp. 285–297, 2001.

[54] A. Syed, M. Izquierdo, P. Rodríguez et al., "A novel experimental investigation of a solar cooling system in Madrid," *International Journal of Refrigeration*, vol. 28, no. 6, pp. 859–871, 2005.

[55] D. Zambrano, C. Bordons, W. Garcia-Gabin, and E. F. Camacho, "Model development and validation of a solar cooling plant," *International Journal of Refrigeration*, vol. 31, no. 2, pp. 315–327, 2008.